Volume 6 | Number 35 | 21 September 2018 | Pages 9279–9570

Journal of Materials Chemistry C

Materials for optical, magnetic and electronic devices

rsc.li/materials-c

ISSN 2050-7526

ROYAL SOCIETY OF CHEMISTRY

PAPER

Pengju Zeng, Zhengchun Peng *et al.*

Efficient deep blue electroluminescence with CIE*y* ∈ (0.05–0.07) from phenanthroimidazole–acridine derivative hybrid fluorophores

Journal of Materials Chemistry C

PAPER

View Article Online
View Journal | View Issue

Cite this: J. Mater. Chem. C, 2018, 6, 9363

Efficient deep blue electroluminescence with CIE*y* ∈ (0.05–0.07) from phenanthroimidazole–acridine derivative hybrid fluorophores†

Shuo Chen, ‡[a] Jiarong Lian,‡[a] Weigao Wang,[b] Yue Jiang,[a] Xuedong Wang,[c] Shuming Chen,[b] Pengju Zeng*[a] and Zhengchun Peng *[a]

Received 16th June 2018,
Accepted 27th July 2018

DOI: 10.1039/c8tc02954g

rsc.li/materials-c

Two bipolar emitters, deep blue phenanthroimidazole derivatives, **PhImAc** and **PhImEn**, were synthesized by incorporating the hole-transporting 9,9-dimethylacridan/9,9-diphenylacridan and electron transporting phenanthroimidazole moieties *via* D–π–A architecture. Both compounds feature Commission International de L'Eclairage (CIE) coordinates of $y < 0.08$ as well as high photoluminescence quantum yields of 0.46 in thin films. Non-doped organic light emitting diodes (OLEDs) with compounds **PhImAc** and **PhImEn** as the emitters were fabricated and exhibited narrow full-width at half-maximum values of 62 nm and 59 nm with the CIE coordinates of (0.15, 0.07) and (0.15, 0.05), respectively, which is very close to the National Television Standards Committee (NTSC) standard blue (0.14, 0.08). The device using the **PhImAc** emitter possesses a favorable maximum efficiency of 3.68% for external quantum efficiency (EQE). When the luminescence reaches 10 000 cd m^{-2}, only a slight roll-off in EQE was observed, *i.e.*, maintaining at 3.01%. The CIE*y* coordinates of the device using the **PhImEn** emitter were among the smallest reported values of non-doped OLEDs. The excellent thermal stability of **PhImAc**/**PhImEn** and the balanced charge transfer performance of our devices demonstrate that both emitters could be alternative host materials in OLED applications. In addition, white organic light-emitting diodes were fabricated using **PhImAc** or **PhImEn** doped with indium phosphor (PO-01), and they showed maximum current efficiency of 19.2 cd m^{-2} and CIE coordinates of (0.34, 0.26). The results of this work have confirmed that the novel phenanthroimidazole–acridine hybrids can not only be used as deep blue emitters, but also have the potential to be excellent hosts for other emitters.

1. Introduction

The field of organic light emitting diodes (OLEDs) has witnessed rapid progress accompanied by successful commercialization in the past few decades. Great efforts have been made to continue improving the external quantum efficiency (EQE) of OLEDs.[1–3] For the pivotal emitting layer in OLEDs, research investigation has gone through three stages: from fluorescent molecules[4] to phosphorescent molecules,[5–9] and to thermally activated delayed fluorescent molecules (TADF).[10–12] Although both phosphorescent and TADF materials can effectively utilize singlet and triple excitons to realize great EQE, some crucial issues remain unresolved: the color range of phosphorescent and TADF devices hardly falls into the region of deep blue, which makes the development of blue OLEDs lags behind their green and red counterparts due to the broad energy gap and balance of carrier injection/transmission. In general, the deep blue refers to the Commission International de L'Eclairage (CIE) coordinates of $y < 0.15$ together with an $(x + y) < 0.30$.[13] Furthermore, in the area of display devices, a higher degree of saturation is necessary for a deeper blue to fulfill the CIE coordinates of high definition television (0.15, 0.06), European Broadcasting Union (0.15, 0.06) and National Television Standards Committee (NTSC) (0.14, 0.08).[14] High energy deep blue emitters could not only effectively reduce the power consumption of the devices, but also be utilized to generate the light of other colors using an energy cascade to lower energy fluorescent or phosphorescent dopants.[15–17] So far, almost all the reported phosphorescent and TADF electroluminescences

[a] Key Laboratory of Optoelectronic Devices and Systems of Ministry of Education and Guangdong Province, College of Optoelectronic Engineering, Shenzhen University, Shenzhen, Guangdong, 518060, P. R. China. E-mail: zcpeng@szu.edu.cn, zengpj@szu.edu.cn; Fax: +86-057-26732932
[b] Department of Electrical and Electronic Engineering, Southern University of Science and Technology, Shenzhen, Guangdong, 518055, P. R. China
[c] Key Laboratory for Carbon-Based Functional Materials and Devices, Institute of Functional Nano and Soft Materials (FUNSOM) of Jiangsu Province, Soochow University, Suzhou, Jiangsu, 215123, P. R. China

† Electronic supplementary information (ESI) available. See DOI: 10.1039/c8tc02954g

‡ These authors contributed equally.

are still rare because of the challenge of obtaining a high EQE at the same time as ensuring a CIEy < 0.08[18–20] or even a CIEy coordinate < 0.06,[21] and which is mainly attributed to the nature of huge energy gap (>2.8 eV) hindering the charge injection and disturbing the balance between hole and electron.[22] To achieve successful commercial OLEDs, there are a variety of constraints that should be considered, such as luminance (stability), fabrication technique, efficiency and atom economy. For example, in 2018, Chan and co-workers obtained deep blue TADF OLEDs based on the carbazole and benzonitrile system,[19] which exhibited the maximum EQE of up to 7.7% at a low current density, and CIE coordinates of (0.15, 0.07). However, the fact that the maximum luminance of these OLEDs are less than 100 cd m^{-2} should not be ignored. Recently, Lu and co-workers reported the deep blue fluorescent OLEDs with phenanthroimidazole (PI) and anthracene moieties, which possessed an EQE of 3.21% at 10 000 cd m^{-2} and CIE coordinates of (0.15, 0.07).[23] It should be noted that the outstanding results are achieved using the doping technique. Yang *et al.* developed a series of blue pyrene-based luminogens, and the corresponding device based on Py-2TF achieved an EQE of 2.1% with CIE coordinates of (0.15, 0.08).[24] Chen *et al.* systematically investigated a series of aromatically substituted phenanthroimidazole fluorophores at C6 and C9, and the EQE of a non-doped OLED using TPI-Ph showed an EQE of 3.72% with CIE coordinates of (0.158, 0.050).[25] The good EQE was realized at the expense of two extra reaction steps. As mentioned previously, the EQEs of OLEDs with CIEy < 0.08 are apparently inferior to those of pure blue OLEDs. Given the limited examples of deep blue OLEDs reported thus far, the development of efficient materials is an essential research goal. In addition, deep blue emitters are also suitable for use as a host material to construct white OLEDs (WOLEDs),[26–28] which was because of its high first triplet energy level fitting the excited level of phosphors and the relative low first singlet energy level for improved and balanced carrier injecting/transporting in emitting layers (EMLs). A prudent strategy for bipolar molecular design does not only decrease the driving voltages but also improves electroluminescent (EL) efficiencies and further eliminates the interface localized recombination zone.[29,30]

Traditional free-transition metal purely organic fluorescent molecules are still used for the design and preparation of deep blue emission because of the bottleneck in design of the commercial OLEDs. However, it is not easy to design a CIEy < 0.08-based emitter with a high quantum yield, at a relatively reasonable cost and with a simple reaction pathway.[31] The scale of the π-conjugated system for the emitter and the electronic effect of substituents are the dominating considerations for determining luminescence properties.[32–34] As is already known, a bulky aromatic coupling system and proper electron-donating or electron-withdrawing substituents on the molecule may give rise to the bathochromic shift of the emission. Therefore, all the factors: relatively short conjugation, twisted steric configuration and weak intermolecular interaction are of great significance and have to be considered. In this paper, two novel fluorescent emitters, deep blue phenanthroimidazole derivatives, **PhImAc** and **PhImEn**, are presented, which are constructed using PI and 9,9-dimethylacridan/9,9-diphenylacridan. Furthermore, the C2 position of the imidazole and the N9 position of the acridine derivatives is linked by the *para* position of a freely rotatable phenyl bridge. The PI skeleton, benefitted from the amine N atom in the imidazole ring as well as a conjugation plane fused by moonlike phenanthrene and imidazole, gives a weak electron donating ability and appropriate highest occupied molecular orbital (HOMO) energy level to reduce the hole injection barrier in the device. Meanwhile, PI derivatives have proven to be promising because of their potential modification site as near the ultraviolet chromophore. The C2,7 or C3,6 positions of the phenanthrene unit provides two sites,[25,35] whereas the C2 or C3 position of the phenanthrene unit provides a single site.[36] The –NH site of the imidazole could deprotonate to connect a wide range of substituents, which are capable of inhibiting strong π–π stacking and molecular interactions in the solid state.[37] The C2 position of the imidazole is able to couple with functional groups to improve the quantum yield and generate a bipolar characteristic.[38] In addition, using acridine derivatives as the donor unit have been frequently adopted to construct TADF molecules in recent years.[39,40] In contrast to the classical carbazole and triphenylamine, acridine possesses a stronger ability for electron-donation and has a deeper HOMO energy level, which favors a hypochromatic shift of emission.[41] Both of the emitters (**PhImAc** and **PhImEn**) were synthesized with a high yield and used to fabricate the deep blue OLED and WOLEDs enabled using non-doping and then used as a host for a yellow emitter, indium phosphor (PO-01), giving a forward viewing maximum EQE of 3.68% with CIE coordinates of (0.15, 0.07), quite small CIEy coordinates of (0.15, 0.05) and an EQE of 10.6% with CIE coordinates of (0.34, 0.26), respectively. It benefited from contributions of the bipolar character and reasonable device architecture, low turn-on voltage and efficient roll-off were achieved, which has motivated the exploration of the utilization of PI derivatives for manufacturing applications.

2. Results and discussion

2.1 Synthesis and characterization

The synthesis route of **PhImAc** and **PhImEn** is shown in Fig. 1. The key intermediate **PhImBr** was first synthesized using a one-pot reaction with 86% yield according to a previous report by Chen *et al.*[42] This was followed by treatment with 9,9-dimethylacridan/9,9-diphenylacridine in the presence of a palladium (Pd)-catalyst, and the target compound, **PhImAc** and **PhImEn** were obtained with about 80% yield. The overall yield of two steps was 70%, which was enough to allow gram scale production. This synthesis method could be conveniently used to construct PI derivatives with various structures by tuning the aromatic aldehyde and the primary amine. The target molecules were obtained using a typical Suzuki cross-coupling reaction, Buchwald–Hartwig reaction or Ullmann reaction between the PI bromide intermediate and the precursors which were boric acid derivatives, boric acid ester derivatives or

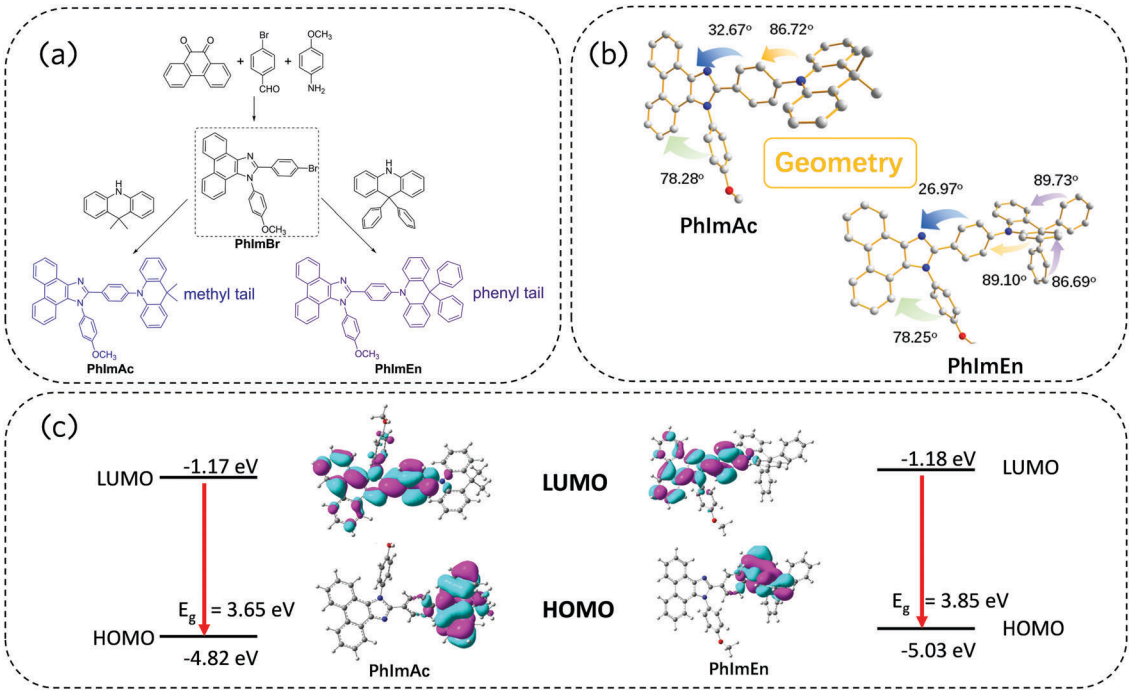

Fig. 1 (a) Synthesis route of emitters **PhImAc** and **PhImEn**. (b) The optimized geometrical configuration. (c) Calculated frontier molecular orbital electron density distribution of emitters **PhImAc** and **PhImEn**.

secondary amine derivatives. Use of proton nuclear magnetic resonance (^{1}H-NMR) and high resolution mass spectroscopy (HR-MS) characterization revealed the intermediates and confirmed that the final products had the correct structure and high purity. Both of the molecules had good solubility in common organic solvents such as tetrahydrofuran, dichloromethane (DCM), chloroform and toluene. The detailed synthetic procedure and analysis are shown in Experimental section.

2.2 Steady-state photophysical properties

The ultraviolet/visible (UV/vis) absorption spectra of **PhImAc** and **PhImEn** were carried out in DCM solution ($c = 1 \times 10^{-5}$ M) at room temperature, as shown in Fig. 2a. The key photophysical data are summarized in Table 1. The electronic absorption spectra of compounds in DCM exhibit moderately intense high energy absorption bands at the range of 225–280 nm (230 nm and 262 nm) and low energy absorption bands at 318 nm and 363 nm. The high energy moderate absorption peak located at 230 nm was assigned to the $\pi \rightarrow \pi^*$ transition of the phenanthrene moiety.[42] The strong absorption bands at around 262 nm originated from the isolated benzene ring connected with imidazole,[43] and the $\pi \rightarrow \pi^*$ transition of acridine (284–341 nm) partially merges with this absorption band.[44] The weak peaks at a high energy of 365 nm originated from an intramolecular charge transfer transition from the electron-donating group to the electron-withdrawing group.[45] Furthermore, the absorption thresholds of **PhImAc** and **PhImEn** were extended to a longer wavelength (approximately 374 nm). The corresponding optical band gaps were estimated to be 3.26 eV and 3.31 eV on the basis of the absorption edge.

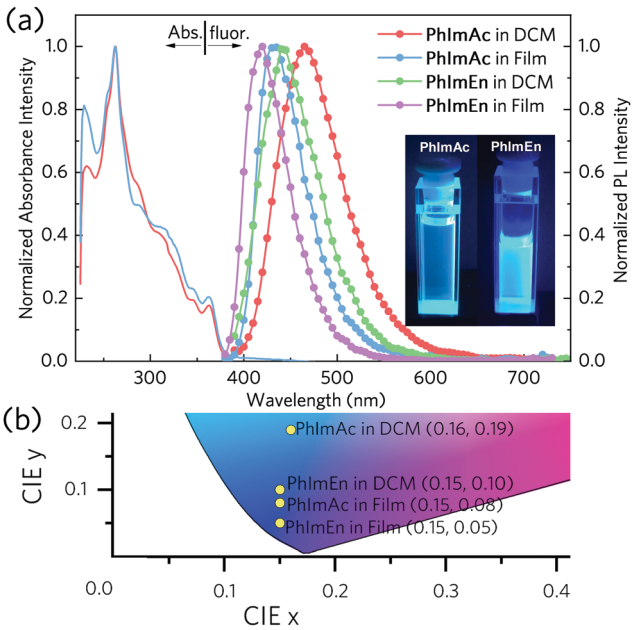

Fig. 2 (a) Steady-state absorption (solid lines) and photoluminescence (symbol lines) spectra of **PhImAc** and **PhImEn** in DCM solvent and in a neat film at room temperature. Inset: Photographs of **PhImAc** and **PhImEn** in DCM under 365 nm hand lamp irradiation. (b) The CIE coordinates of **PhImAc** and **PhImEn**.

The peaks of the photoluminescent (PL) emissions of **PhImAc** and **PhImEn** were observed at 466 nm and 435 nm, respectively. The bathochromic shift of 31 nm was primarily because of the steric hindrance of the phenyl group. Compared with that of PL

Table 1 The photophysical and thermal properties of **PhImAc** and **PhImEn**

Compound	$\lambda_{max,abs}$[a] [nm]	Fluorescence				PLQY[c]	E_S[d]/E_T[e]/ΔE_{ST}	T_g[f]/°C	T_d[g]/°C	HOMO		LUMO		E_g	
		λ_{max}[a] [nm]	FWHM[b] [nm]	λ_{max}[c] [nm]	FWHM[b] [nm]					Calculated[h] [eV]	Measured[i] [eV]	Calculated[h] [eV]	Measured[j] [eV]	Calculated[h] [eV]	Measured[k] [eV]
PhImAc	231, 262, 311, 363	465	81	442	74	0.46	2.99/2.52/0.47	140	328	4.82	5.27	1.17	2.01	3.65	3.26
PhImEn	229, 262, 315, 363	432	61	419	54	0.28	3.13/2.55/0.58	—	454	5.03	5.34	1.18	2.03	3.85	3.31

[a] Measured in DCM solution at room temperature. [b] Full-width at half-maximum. [c] Measured in the vacuum evaporated film at room temperature. [d] Estimated according to the PL spectra in toluene solution. [e] Determined from the highest energy vibronic peaks of phosphorescence spectra measured in toluene at 77 K. [f] T_g: glass transition temperature, obtained from DSC measurements. [g] T_d: decomposition temperature at weight loss of 5%, obtained from TGA measurements. [h] Calculated from DFT at the B3LYP/6-31G(d) level. [i] HOMO was measured from the onset value of the oxidation potential. [j] LUMO was measured from the HOMO and the optical band gap E_g. [k] E_g: the optical band gap was calculated from the absorption spectra.

measured in DCM, the neat films of **PhImAc** and **PhImEn** exhibited hypochromatic shift emission in the deeper blue region with peaks at 442 nm and 419 nm, respectively. The corresponding CIE coordinates of **PhImAc** and **PhImEn** were (0.16, 0.08) and (0.15, 0.05), respectively. With increasing solvent polarity (Fig. S8, ESI†), the emission spectra gradually broadened and showed a bathochromic shift from 388 nm in *n*-hexane to 467 nm in dimethylformamide (DMF) for **PhImAc**, and from 382 nm in *n*-hexane to 445 nm in DMF for **PhImEn**. Such solvatochromic behavior demonstrates the existence of a charge transfer moiety in the excited state. Fig. S9 (ESI†) shows the phosphorescence spectra of **PhImAc** and **PhImEn** in toluene at 77 K, which reveals well-structured emission bands with the highest energy vibronic peaks at 492 nm and 487 nm, and the triplet energies (E_T) of 2.52 eV and 2.55 eV were determined for **PhImAc** and **PhImEn**, respectively. Furthermore, the singlet–triplet energy gaps (ΔE_{ST}) were calculated to be 0.47 and 0.58 eV for **PhImAc** and **PhImEn**, respectively, which was much higher than that of the TADF materials, thus, both of the emitters could be regarded as having fluorescence featured emissions. High photoluminescence quantum yield (PLQY) was vital to evaluate the device performance of the non-doped OLEDs. The PLQYs of **PhImAc** and **PhImEn** were measured using the vacuum evaporated film (100 nm), which gave the values of 0.46 and 0.28, respectively. The decreased PLQY of **PhImEn** demonstrated that the phenyl-tail could induce intermolecular interaction and PL quenching. The high PLQY suggested that both emitters would be promising candidates for high performance deep blue OLEDs.

2.3 Thermal properties

Thermogravimetric analysis (TGA) as well as differential scanning calorimetry (DSC) were performed to investigate the thermal properties of both emitters. The curves were shown in Fig. S10 (ESI†). **PhImEn** exhibited a high thermal stability with a weight loss of 5% at the temperature of 454 °C, whereas **PhImAc** had a lower decomposition temperature (T_d) of 328 °C, which was ascribed to the higher rigidity of the phenyl substituents. The glass transition temperature (T_g) of the **PhImAc** was found to be 140 °C. The T_g of **PhImEn** was not observed under the operating temperature from 25 °C to 250 °C, which indicated that **PhImEn** can retain its amorphous morphology under a wide range of temperatures and can be expected to decrease the phase separation rate of the guest–host system.[17]

2.4 Theoretical calculations

Further insight into the molecular orbital distributions of both materials was gained by using density functional theory (DFT) calculations, which were carried out at the level of the Lee–Yang–Parr functional (B3LPY)/6-31(d) basis to investigate their ground states. Fig. 1b shows the minimized energy structure of **PhImAc** and **PhImEn** in the gas phase. The conformation of two molecules was similar with nearly orthogonal geometries between the Ac and phenyl units ($\theta_{D-\pi}$ = 87°–89°), whereas the dihedral angles between the phenyl and PI of **PhImAc** and **PhImEn** were found to be 33° and 27°, respectively. The difference between

the two molecules could be attributed to the configuration variations of the terminal group. In comparison to methyl-tailed **PhImAc**, two bulky phenyl groups of **PhImEn** with a perpendicular steric configuration could effectively suppress the formation of coplanar aggregation. The multiple twisted architecture could prevent the formation of excimers and exciplexes in the solid state. Meanwhile, the twisted structure contributed significantly to achieve an effective separation between the HOMO and the lowest unoccupied molecular orbital (LUMO), as shown in Fig. 1c. Showing a similar distribution pattern, the HOMOs of **PhImAc** and **PhImEn** were distributed on an electron rich acridine moiety. Whereas, the electron distributions of the corresponding LUMOs were dominantly localized on the electron deficient phenanthroimidazole and extended to the benzene ring with little residual from the acridine part. Therefore, a typically observable extensive HOMO–LUMO separation and little HOMO–LUMO overlap at the phenyl segment were apparent in the molecular orbital diagram. The almost complete spatial separation of the HOMO and LUMO energy level suggests that the HOMO–LUMO excitation would shift the electron density distribution from one side of the donor acridine to the other side of the acceptor phenanthroimidazole, leading to a polarized excited state. It is essential that such a separation of the electron cloud of HOMO and LUMO could give the transport channels between the hole and the electron, which may give the molecules the ability effect bipolar charge transport.

2.5 Electrochemical properties

To better understand the electron structure (HOMO and LUMO) of the two compounds, the electrochemical behaviors were evaluated using cyclic voltammetry (CV) analysis to determine the optoelectronic applications. As shown in Fig. S11 (ESI†), **PhImAc** and **PhImEn** exhibit one quasi-reversible oxidation wave with an oxidative onset potential of 0.47 eV and 0.63 eV compared to ferrocene. The threshold of the oxidation potential increases with the decreasing electron donating strength. The HOMO levels were calculated according to the equation $E_{HOMO} = [E_{onset,ox} + 4.8]$ eV. The LUMO levels were calculated using subtraction of the optical energy gap (E_g) from the HOMO energy levels. The relevant energy level data are also listed in Table 1. The HOMO energies of **PhImAc** and **PhImEn** were −5.27 eV and −5.34 eV, respectively. By subtracting of the optical energy band gaps from the HOMO energy levels, the LUMO energy levels of **PhImAc** and **PhImEn** were calculated to be −2.01 eV and −2.03 eV, respectively.

2.6 Electroluminescent properties

Inspired to further investigate the potential applications of the deep blue OLED, multilayer OLEDs with the classical configurations of indium tin oxide (ITO)|HAT-CN (15 nm)|TAPC (40 nm)|**PhImAc** (device A) or **PhImEn** (device B) (30 nm)|TmPyPB (40 nm)|LiF (1 nm)|Al (100 nm) were fabricated, where hexaazatriphenylenehexacabonitrile (HAT-CN) and lithium fluoride (LiF) were used as an anode/cathode buffer layer for hole/electron injection, respectively. The 4,4′-cyclohexylidenebis[*N*,*N*′-bis(4-methylphenyl)aniline] (TAPC) acted as hole-transport layers. The 1,3,5-tri[(3-pyridyl)-phen-3-yl]benzene (TmPyPB) is used as the electron-transport, hole-blocking and exciton-blocking layers. The energy level diagram of devices A and B is shown in Fig. 4a.

As displayed in Fig. 3a and c, non-doped devices using the **PhImAc** or **PhImEn** as the EMLs show maximum peaks at 431 nm and 415 nm with the CIE coordinates of (0.15, 0.07) and (0.15, 0.05), respectively. The observed CIE coordinates are very close to the standard values suggested by NSTC blue (0.14, 0.08). Neither of the EL spectra has a vibronic feature and coincides with the PL spectra in the thin film, which implies effective charge injection and recombination in the EML. More importantly, the saturated deep blue EL emissions were quite stable under the applied voltages ranging from 6 V to 10 V (Fig. 3b and d). Through a more detailed analysis of the energy level diagram, it was found that the hole injection barrier at TAPC/EML was 0.03 eV and the electron injection barrier at TmPyPB/EML was non-negligible at 1.0 eV. Such energy levels would seem to promote hole injection and transportation. However, TmPyPB has a better of electron mobility capability and hole blocking than the traditional electron transport layer (ETL) material, 2,2′,2″-(1,3,5-benzinetriyl)-tris(1-phenyl-1-*H*-benzimidazole) (TPBi), although the LUMO of TPBi (2.7 eV) was shallower than that of TmPyPB. As summarized in Table 2, the lower driving voltage of 3.3 V for the onset of device B compared to that of device A (4.1 V) was realized because of the well matched HOMO/LUMO levels between the EML and the transport layers. The devices A and B delivered a maximum EQE of 3.68% and 2.50%, respectively. It is worth noting that the EQE of device A went through an uphill process before reaching 1000 cd m^{-2} and then there is a slight roll-off afterwards. The efficiency roll-off of device A was quite slight even under the luminescence of 10 000 cd m^{-2}, the EQE still remains at 3.01% (Fig. 4c), which was ascribed to the singlet excitons not being severely quenched with the increasing current density. It should be noted that, both devices performed with a high EQE_{max} using emitters with medium PL efficiency, which was the result of the enhanced light out-coupling effect.[46] However, the optical microcavity effect should be considered, which can be suggested by the obvious narrowing of the spectrum from the PL spectrum for **PhImAc** film to that of the EL spectrum for OLEDs (the FWHM of the spectrum change from 74 nm to 62 nm). Alternatively, the horizontal orientation of the transition dipole moments in the EL favors light out-coupling enhancement.[47] Here **PhImAc** and **PhImEn** have the same donor units and a large twisted angle of chemical structure with the typical horizontal emitters of *N*,*N*-dimethylacetamide (NAI-DMAC) and *N*,*N*-diphenylacetamide (NAI-DPAC).[3] As far as was known, the EQE of device A was superior to that of most of the reported deep blue devices with a CIEy < 0.08 at high luminescence of 10 000 cd m^{-2},[16,48] which suggests that the acridine unit was an excellent building block that was capable of being used to construct deep blue emission molecules. The device based on **PhImEn** possessed an EQE_{max} of 2.50% and CIE coordinates of (0.15, 0.05), which was one of the smallest CIEy values so far reported in deep blue OLEDs.[21,49,50]

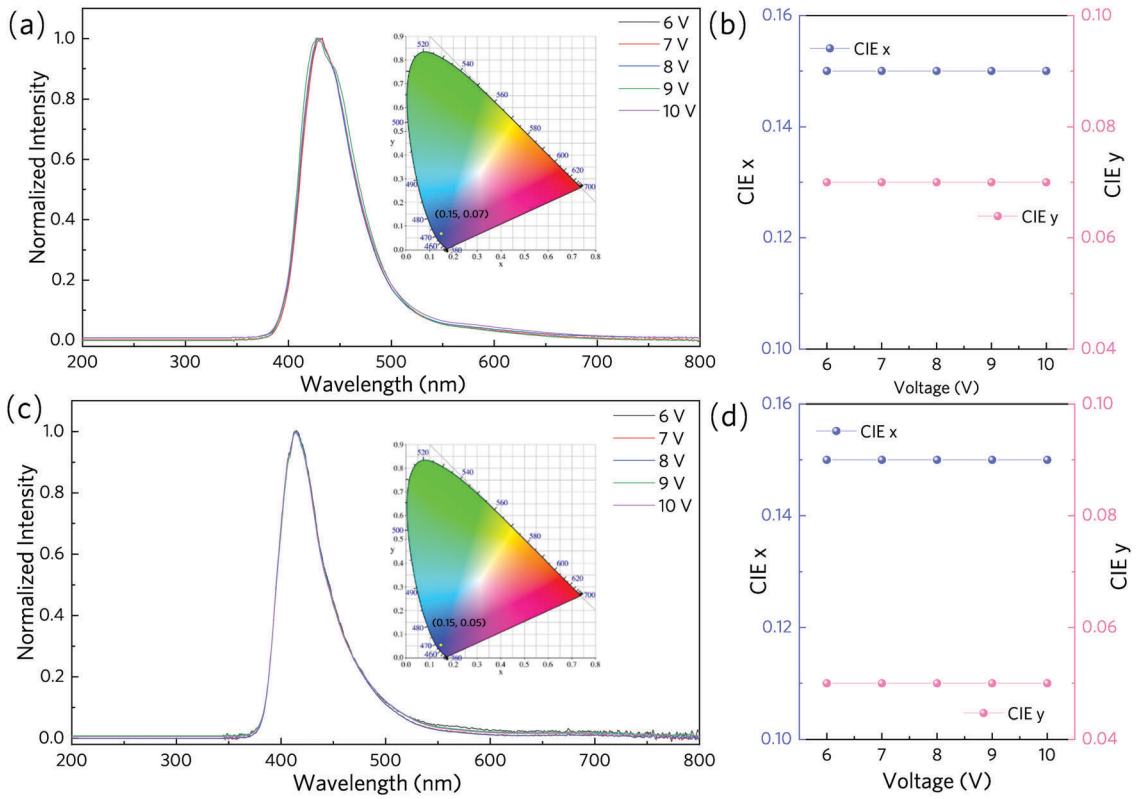

Fig. 3 (a) Electroluminescence spectra for deep blue devices A. Inset: CIE coordinates of device A. (b) CIE coordinates of device A at different voltages. (c) Electroluminescence spectra for deep blue devices B. Inset: CIE coordinates of device B. (d) CIE coordinates of device B at different voltages.

Table 2 EL performance of deep blue devices A and B and white devices C and D

Device	Emitter	V_{on}[a] (V)	λ_{max} (nm)	Luminance (cd m^{-2})	FWHM (nm)	CE_{max}[b] (cd A^{-1})	PE_{max}[b] (lm W^{-1})	EQE_{max}[b] (%)	CIE (x, y)[c]	CRI[d] at 6–10 V
A	**PhImAc**	4.1	431	20 678	62	3.65	2.01	3.68	(0.15, 0.07)	—
B	**PhImEn**	3.3	414	11 696	59	2.30	1.32	2.50	(0.15, 0.05)	—
C	**PhImAc** + PO-01	4.3	430, 568, 601^{sh}	28 143	—	9.04	5.46	5.25	(0.33, 0.26)	62–55
D	**PhImEn** + PO-01	3.5	412, 565, 602^{sh}	19 050	—	19.2	14.8	10.6	(0.43, 0.36)	59–57

[a] Voltage required for 1 cd m^{-2}. [b] Current efficiency (CE_{max}), power efficiency (PE_{max}), external quantum yield (EQE_{max}). [c] The CIE are measured at 1000 cd m^{-2}. [d] Color rendering index. sh: shoulder.

To further understand both the hole/electron injection and transport properties, single-carrier devices were fabricated using the following configuration: the nominal hole only and electron only devices were fabricated with the structures: ITO|HAT-CN (10 nm)|TAPC (10 nm)|**PhImAc** or **PhImEn** (120 nm)|TAPC (10 nm)|HAT-CN (10 nm)|Al (100 nm) (hole only transporting device) and ITO|LiF (1 nm)|TmPyPB (20 nm)|**PhImAc** or **PhImEn** (120 nm)|TmPyPB (20 nm)|LiF (1 nm)|Al (100 nm) (electron only transporting device). TAPC and TmPyPB were used to prevent electron and hole injection from cathode and anode, respectively. The current density *versus* voltage curves of the devices are shown in Fig. 5a. In general, the mobilities of the hole were two or three orders of magnitude higher than those of the electron in organic semiconducting materials. Carrier mobilities were evaluated using a space-charge-limited current (SCLC) method based on current density–voltage (J–V) measurements of single-carrier devices. The hole and electron mobility can be calculated by combining the Mott–Gurney equation and Frenkel effect (Fig. 5b). The Mott–Gurney is expressed as eqn (1):

$$J = \frac{9}{8}\varepsilon_0\varepsilon_r\mu_0\frac{E^2}{L}\exp\left(\gamma\sqrt{E}\right) \quad (1)$$

where J is the measured current density, ε_0 is the freespace dielectric constant ($\varepsilon_0 = 8.85 \times 10^{-14}$ C V^{-1} cm^{-1}), μ_0 is the zero-field carrier mobility, E is the electric field intensity, L is the thickness of active layer, γ is the field-activation factor, and ε_r is the relative permittivity (assumed to be 3.0). Thus, the hole mobility was calculated to be 1.24×10^{-5} cm^2 V^{-1} s^{-1} and 4.24×10^{-5} cm^2 V^{-1} s^{-1} for **PhImAc** and **PhImEn**, respectively. The electron mobilities were calculated to be 5.16×10^{-6} cm^2 V^{-1} s^{-1} and 4.60×10^{-6} cm^2 V^{-1} s^{-1} for **PhImAc** and **PhImEn**, respectively. The hole mobilities of **PhImAc** and **PhImEn** were approximately one order of magnitude higher than those of the electron mobility,

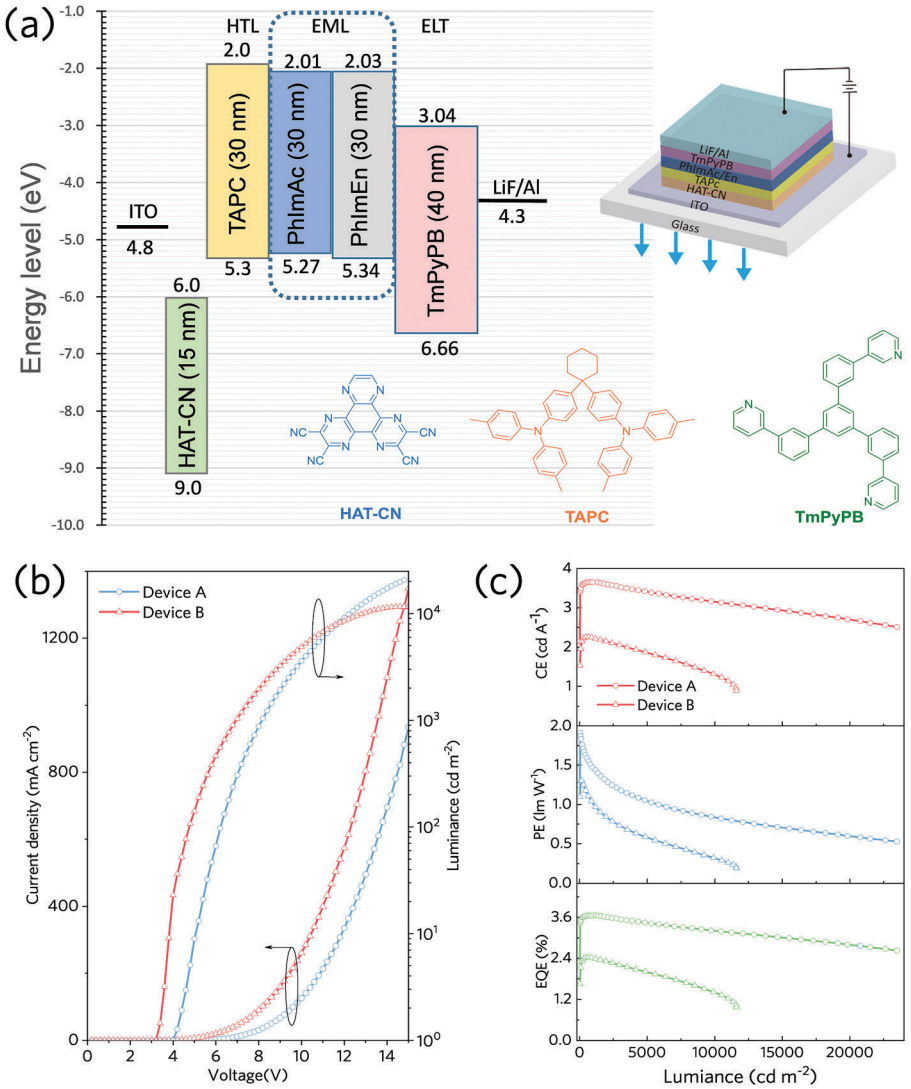

Fig. 4 (a) Energy level diagrams of devices A and B based on **PhImAc** and **PhImEn**, respectively, as the EML. (b) Current density–voltage–luminance characteristics for devices A and B. (c) Efficiency *versus* luminance curves of non-doped devices based on **PhImAc** and **PhImEn**.

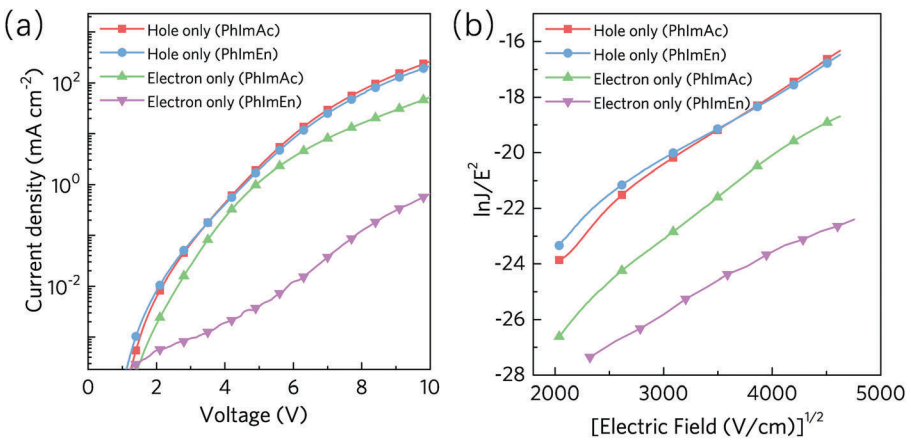

Fig. 5 (a) Current density *versus* voltage characteristics of the hole only and electron only devices for **PhImAc** and **PhImEn**. (b) Hole and electron mobilities of **PhImAc** and **PhImEn** estimated using the SCLC method.

which undoubtedly shows the balanced bipolar charge transport capacity. Furthermore, the electron mobilities of **PhImAc** were higher than those of **PhImEn**, which was probably caused by the molecule packing and was morphology dependent for **PhImEn**. Therefore, **PhImAc** has a more balanced bipolar charge transporting capacity as shown by the balanced hole/electron mobility, as a result, the results showed that the device performance of **PhImAc** was superior to that of the **PhImEn**. All these results lead to the conclusion that **PhImAc** and **PhImEn** were excellent bipolar materials, which could be used as non-doped deep blue OLEDs.

WOLEDs are tremendously significant because their application in the field of backlights and solid-state lighting sources. In principle, two complementary colors, as long as the connection line lies across the white light region, could generate white light. Therefore, the deep blue emitters of **PhImAc** or **PhImEn** should match yellow light emitting molecules to give to white light. Based on this **PhImAc** or **PhImEn** were further utilized as the hosts for [acetylacetonatobis(4-phenylthieno[3,2-*c*]pyridinato-*N*,*C*2′) iridium] (PO-01) to fabricate the fluorescence–phosphorescence hybrid WOLEDs with the configuration of ITO|HAT-CN (15 nm)|TAPC (30 nm)|EML|TmPyPB (40 nm)|LiF (1 nm)|Al (100 nm). By precisely tuning the ratio between the deep blue emitter and yellow PO-01, the dopant PO-01 was chosen to be introduced into **PhImAc** or **PhImEn** in a very thin thickness of 0.3 nm to give the EML a sandwich-style structure, as shown in Fig. S12 (ESI†). The typical EL spectra of the WOLEDs at different voltages are shown in Fig. S13a (ESI†). The dual emission EL spectra could be divided into their blue emission corresponding to the fluorophores **PhImAc** or **PhImEn** and yellow emission (556 nm) corresponding to the phosphor PO-01. The CRIs range from 62 at 6 V to 55 at 10 V for device A and 59 at 6 V to 57 at 10 V for device B. As shown in Table 2, the maximum forward-viewing current efficiencies of 9.04 cd m^{-2}, 19.2 cd A^{-1}, power efficiencies of 5.46 lm W^{-1}, 14.8 lm W^{-1} and EQE values of 5.25%, 10.6% were achieved, based on the **PhImAc** or **PhImEn**, respectively, and PO-01 without using any light out-coupling technology. In contrast to the fact that the fluorescent material contributing to the high efficiency of the deep blue devices, the high efficiency of our fluorescence-phosphorescence hybrid WOLED was mostly contributed by the phosphorescent dopant material PO-01.

3. Experimental sections

3.1 Materials and instruments

All the reagents and solvents used for the synthesis were purchased from Sigma-Aldrich, J&K Scientific and TCI Chemicals and were used as received. Dopant material (PO-01) was purchased from Lumtec (Taiwan). The ^{1}H-NMR spectra were recorded using a Bruker AVANCE III 500 MHz spectrometer or a Bruker 600 MHz spectrometer, using deuterated chloroform ($CDCl_3$) as the solvent and tetramethylsilane (TMS) as the internal standard. The HR-MS spectra were recorded on an AB SCIEX 5800 matrix-assisted laser desorption ionization-time-of-flight/time-of-flight (MALDI-TOF/TOF) spectrometer. Elemental analysis for carbon, hydrogen and nitrogen (C, H and N) were performed on an Elementar Analysensysteme elemental analysis instrument. All the manipulations involving air sensitive reagents were performed in an atmosphere of dry argon. Absorption and PL emission spectra of the target compound were measured using a PerkinElmer Lambda 750 ultraviolet-visible-near infrared (UV-vis-NIR) spectrophotometer and a PerkinElmer LS 55 fluorescence spectrometer, respectively. For the solid samples, the quantum yields for the compounds were determined at room temperature using an absolute method with an Edinburgh Instruments' integrating sphere coupled to a modular Edinburgh Instruments FLS920 fluorescence spectrophotometer. The values reported are the average of three independent determinations for each sample. The absolute quantum yield was calculated using the eqn (2):

$$\Phi = \frac{\int L_{\text{emission}}}{\int E_{\text{reference}} - \int E_{\text{sample}}}. \quad (2)$$

In eqn (2), L_{emission} is the emission spectrum of the sample, collected using the sphere, E_{sample} is the spectrum of the incident light used to excite the sample, collected using the sphere, and $E_{\text{reference}}$ is the spectrum of the light used for excitation with only the reference in the sphere. The method was accurate to within 10%. The TGA and DSC were performed on a PerkinElmer TGA 4000 and a PerkinElmer DSC 8000 thermal analyzer under a nitrogen atmosphere at a heating rate of 10 °C min^{-1}. The CV measurements were carried out in a conventional three electrode cell using a platinum (Pt) button working electrode of 2 mm in diameter, a Pt wire counter electrode, and a saturated calomel electrode reference electrode on a computer controlled CH Instruments CHI660d electrochemical workstation at room temperature. Reduction CV of all the compounds was performed in DCM containing tetrabutylammonium hexafluorophosphate (Bu_4NPF_6, 0.1 M) as the supporting electrolyte. Ferrocene was used as an external standard. Electrochemistry was done at a scan rate of 100 mV s^{-1}.

3.2 Computational details

The theoretical investigation of the geometry optimization was performed using the Gaussian 09 software program.[51] The DFT calculations were done using the Becke three-parameter hybrid exchange functional[52] and the Lee, Yang and Parr correlation functional[53] B3LYP/6-31G(d). The spin density distributions were visualized using Gaussview 5.0.8 software.

3.3 Device fabrication and measurement

Prior to the device fabrication, the patterned ITO-coated glass substrates were scrubbed and cleaned ultrasonically with detergent water, then deionized water, and finally acetone, before drying in a drying cabinet, and then exposed to a UV-ozone environment for 30 min. After these processes, the substrates were transferred into a vacuum chamber for sequential deposition of all the organic layers using thermal evaporation with a base pressure ($\sim 4.0 \times 10^{-4}$ Pa) at a rate of 0.1–0.2 nm s^{-1} monitored *in situ* with a quartz oscillator. The LiF covered by aluminium (Al) was used as cathode without breaking the vacuum.

All the samples were measured directly after fabrication without encapsulation at room temperature under an ambient atmosphere. The current–voltage–luminance characteristics were determined using a Photo Research PR655 SpectraScan spectrometer and a Keithley 2400 programmable voltage–current source. The EQE and luminous efficiency (LE) were calculated assuming a Lambertian distribution, and then calibrated using the efficiencies obtained at 1000 cd m^{-2} in the integrating sphere (Model: Jm-3200).

3.4 Synthesis

Synthesis of 2-(4-bromophenyl)-1-(4-methoxyphenyl)-1*H*-phenanthro[9,10-*d*]imidazole (PhImBr). A mixture of 4-bromobenzaldehyde (248.3 mg, 13.5 mmol), phenanthrene-9,10-dione (280.9 mg, 13.5 mmol), 4-methoxy-anilin (830.7 mg, 67.5 mmol), ammonium acetate (354.2 mg, 54.5 mmol), and acetic acid (60 mL) were heated under nitrogen at 120 °C for 24 h. After cooling, the mixture was filtered and the precipitate was washed with an acetic acid/water mixture (1 : 1, 100 mL) and water. The solid product was dried *in vacuo* and was then purified by chromatography using DCM/petroleum ether (1 : 1) as an eluent to obtain the product as a green powder. Yield: 70%. ^{1}H-NMR (TMS, $CDCl_3$, 500 MHz): ppm δ = 3.96 (s, 3H), 7.10 (d, J = 8.5 Hz, 2H), 7.29 (t, J = 7.0 Hz, 2H), 7.39–7.45 (m, 4H), 7.48–7.53 (m, 3H), 7.65 (t, J = 8.5 Hz, 1H), 7.73 (t, J = 7.0 Hz, 1H), 8.70 (d, J = 8.0 Hz, 1H), 8.76 (d, J = 8.5 Hz, 1H), 8.84 (d, J = 9.0 Hz, 1H); high resolution-electrospray ionization-mass spectrometry (HR-ESI-MS): $[M + H]^+$ m/z calcd for $C_{28}H_{20}BrN_2O$: 479.07535, found: 479.07449.

Synthesis of 2-(4-(9,9-dimethylacridin-10(9*H*)-yl)phenyl)-1-(4-methoxyphenyl)-1*H*-phenanthro[9,10-*d*]imidazole (PhImAc). **PhImBr** (0.96 g, 2 mmol), 9,9-dimethylacridan (0.42 g, 2 mmol), and potassium *tert*-butoxide (^{t}BuOK; 0.95 g, 6.9 mmol) were placed in a round-bottomed flask. Xylene (30 mL) was added, and nitrogen was bubbled through the mixture for 1 h. Palladium(II) acetate [$Pd(OAc)_2$; 22.5 mg, 0.1 mmol] and tri-*tert*-butylphosphine [$P(^tBu)_3$; 60.7 mg, 0.3 mmol] were then added and the resultant mixture was stirred overnight at 130 °C under a nitrogen flow. The precipitate was filtered off, and the filtrate was washed with brine, dried over anhydrous sodium sulfate (Na_2SO_4), filtered, and concentrated to dryness. The resulting solid was purified using chromatography on silica gel (eluent : ethyl acetate (EtOAc)/hexane, 1 : 5) to give **PhImAc** (0.98 g, 81%) as a white solid. ^{1}H-NMR (600 MHz, $CDCl_3$): δ = 8.91 (s, 1H), 8.80 (d, J = 8.4 Hz, 1H), 8.73 (d, J = 8.4 Hz, 1H), 7.90 (s, 2H), 7.78 (s, 1H), 7.69 (s, 1H), 7.55 (s, 1H), 7.51 (d, J = 9.0 Hz, 1H), 7.45 (d, J = 7.2 Hz, 2H), 7.36–7.30 (m, 4H), 7.15 (d, J = 8.4 Hz, 2H), 6.99–6.92 (m, 4H), 3.97 (s, 3H), 1.67 (s, 6H); MALDI-TOF: m/z calcd for $C_{43}H_{33}N_3O$: 609.27; found: 609.62; elemental analysis calcd (%) for $C_{43}H_{33}N_3O$: C 84.98, H 5.47, N 6.91; found: C 85.06, H 5.34, N 6.85.

Synthesis of 2-(4-(9,9-diphenylacridin-10(9*H*)-yl)phenyl)-1-(4-methoxyphenyl)-1*H*-phenanthro[9,10-*d*]imidazole (PhImEn). The procedure for synthesis of **PhImEn** was similar to the preparation of **PhImAc** except that the starting compound was 9,9-diphenylacridan (0.67 g, 2 mmol) instead of 9,9-dimethylacridan to yield a light white powder in 77% (1.13 g) isolation yield. ^{1}H-NMR (600 MHz, $CDCl_3$): δ = 8.92 (s, 1H), 8.81 (d, J = 8.4 Hz, 1H), 8.74 (d, J = 8.4 Hz, 1H), 7.83 (d, J = 7.2 Hz, 2H), 7.78 (s, 1H), 7.69 (s, 1H), 7.56 (s, 1H), 7.49 (d, J = 8.4 Hz, 2H), 7.34 (t, J = 7.8 Hz, 1H), 7.27–7.22 (m, 7H), 7.14 (d, J = 8.4 Hz, 2H), 7.08–7.05 (m, 4H), 7.00 (d, J = 6.6 Hz, 4H), 6.91 (s, 4H), 6.43 (d, J = 7.8 Hz, 2H), 3.99 (s, 3H); MALDI-TOF: m/z calcd for $C_{53}H_{37}N_3O$: 734.30; found: 734.45; elemental analysis calcd (%) for $C_{53}H_{37}N_3O$: C 86.98, H 5.10, N 5.74; found: C 85.86, H 5.22, N 5.84.

4. Conclusions

In summary, two phenanthroimidazole-based derivatives, **PhImAc** and **PhImEn**, were designed and synthesized. Phenanthroimidazole has been proved to have great potential for building deep blue emitters with a bipolar nature. In particular, different tailed (methyl or phenyl) acridine derivatives further influence the optical and electrical properties, which enables the hypochromatic shift of emission. Simultaneously, weak π–π stacking and molecular aggregation renders good thermal properties and a high photoluminescence quantum yield of 0.46 at room temperature in the solid state. Not only have **PhImAc** and **PhImEn** been used as an emitter to fabricate a deep violet-blue colored OLED, but also as host materials to construct highly efficient WOLEDs. Utilizing **PhImAc** and **PhImEn** as the non-doped emitters in the multilayer devices, the high performance of 3.68% EQE and deep blue CIE coordinates of (0.15, 0.07) were achieved. These values were very close to the NTSC blue criterion (0.14, 0.08). Even when the luminescence reached 10 000 cd m^{-2}, the EQE of these devices was still as high as 3.01%. In particular, devices using **PhImEn** produced CIE coordinates of (0.15, 0.05), which was among one of the smallest CIEy values yet reported in the deep blue OLED field. In addition, doped WOLED with CIE coordinates of (0.43, 0.36) demonstrated a series of high performances, including 19.2 cd A^{-1} for CE, 14.8 lm W^{-1} for PE, 10.6% for EQE and 3.5 V for onset voltage, and it possessed good color stability under a broad range of luminance. It is believed that this work provides novel approaches for realizing deep blue fluorescent and white fluorescence–phosphorescence hybrid OLEDs with high performance.

Conflicts of interest

There are no conflicts to declare.

Acknowledgements

This study was supported financially by the China Postdoctoral Science Foundation (2017M622768), the Basic Research Programs of Shenzhen Science and Technology Innovation Commission (JCYJ20170302153341980, JCYJ20160427161937700, JCYJ20170818091233245), and the Applied Research Program of Department of Education of Guangdong Province (2016KZDXM005).

Notes and references

1 K. T. Ly, R.-W. Chen-Cheng, H.-W. Lin, Y.-J. Shiau, S.-H. Liu, P.-T. Chou, C.-S. Tsao, Y.-C. Huang and Y. Chi, *Nat. Photonics*, 2017, **11**, 63.
2 Y. Wada, S. Kubo and H. Kaji, *Adv. Mater.*, 2018, **30**, 1705641.
3 W. X. Zeng, H. Y. Lai, W. K. Lee, M. Jiao, Y. J. Shiu, C. Zhong, S. L. Gong, T. Zhou, G. H. Xie, M. Sarma, K. T. Wong, C. C. Wu and C. L. Yang, *Adv. Mater.*, 2018, **30**, 1704961.
4 J. N. Moorthy, P. Venkatakrishnan, D. F. Huang and T. J. Chow, *Chem. Commun.*, 2008, 2146.
5 K.-H. Kim, S. Lee, C.-K. Moon, S.-Y. Kim, Y.-S. Park, J.-H. Lee, J. Woo Lee, J. Huh, Y. You and J.-J. Kim, *Nat. Commun.*, 2014, **5**, 4769.
6 X. Yang, B. Jiao, J.-S. Dang, Y. Sun, Y. Wu, G. Zhou and W.-Y. Wong, *ACS Appl. Mater. Interfaces*, 2018, **10**, 10227.
7 Z. Chen, L. Wang, S. Su, X. Zheng, N. Zhu, C.-L. Ho, S. Chen and W.-Y. Wong, *ACS Appl. Mater. Interfaces*, 2017, **9**, 40497.
8 B. Liu, F. Dang, Z. Feng, Z. Tian, J. Zhao, Y. Wu, X. Yang, G. Zhou, Z. Wu and W.-Y. Wong, *J. Mater. Chem. C*, 2017, **5**, 7871.
9 C.-L. Ho and W.-Y. Wong, *New J. Chem.*, 2013, **37**, 1665.
10 S. Hirata, Y. Sakai, K. Masui, H. Tanaka, S. Y. Lee, H. Nomura, N. Nakamura, M. Yasumatsu, H. Nakanotani, Q. Zhang, K. Shizu, H. Miyazaki and C. Adachi, *Nat. Mater.*, 2015, **14**, 330.
11 H. Uoyama, K. Goushi, K. Shizu, H. Nomura and C. Adachi, *Nature*, 2012, **492**, 234.
12 Q. Zhang, B. Li, S. Huang, H. Nomura, H. Tanaka and C. Adachi, *Nat. Photonics*, 2014, **8**, 326.
13 M. R. Zhu and C. L. Yang, *Chem. Soc. Rev.*, 2013, **42**, 4963.
14 T. Shan, Y. L. Liu, X. Y. Tang, Q. Bai, Y. Gao, Z. Gao, J. Y. Li, J. Deng, B. Yang, P. Lu and Y. G. Ma, *ACS Appl. Mater. Interfaces*, 2016, **8**, 28771.
15 K. S. Yook and J. Y. Lee, *Adv. Mater.*, 2012, **24**, 3169.
16 Z. Gao, Z. M. Wang, T. Shan, Y. L. Liu, F. Z. Shen, Y. Y. Pan, H. H. Zhang, X. He, P. Lu, B. Yang and Y. G. Ma, *Org. Electron.*, 2014, **15**, 2667.
17 Y. Li, X. L. Li, X. Cai, D. Chen, X. Liu, G. Xie, Z. Wang, Y. C. Wu, C. C. Lo, A. Lien, J. Peng, Y. Cao and S. J. Su, *J. Mater. Chem. C*, 2015, **3**, 6986.
18 R. J. Holmes, S. R. Forrest, T. Sajoto, A. Tamayo, P. I. Djurovich, M. E. Thompson, J. Brooks, Y.-J. Tung, B. W. D'Andrade, M. S. Weaver, R. C. Kwong and J. J. Brown, *Appl. Phys. Lett.*, 2005, **87**, 243507.
19 C. Y. Chan, L. S. Cui, J. U. Kim, H. Nakanotani and C. Adachi, *Adv. Funct. Mater.*, 2018, **28**, 1706023.
20 T. Fleetham, G. Li, L. Wen and J. Li, *Adv. Mater.*, 2014, **26**, 7116.
21 Z. Gao, Y. L. Liu, Z. M. Wang, F. Z. Shen, H. Liu, G. N. Sun, L. Yao, Y. Lv, P. Lu and Y. Ma, *Chem. – Eur. J.*, 2013, **19**, 2602.
22 J. Zhang, D. Ding, Y. Wei, F. Han, H. Xu and W. Huang, *Adv. Mater.*, 2016, **28**, 479.
23 X. Tang, Q. Bai, T. Shan, J. Li, Y. Gao, F. Liu, H. Liu, Q. Peng, B. Yang, F. Li and P. Lu, *Adv. Funct. Mater.*, 2018, **28**, 1705813.
24 J. Yang, L. Li, Y. Yu, Z. Ren, Q. Peng, S. Ye, Q. Li and Z. Li, *Mater. Chem. Front.*, 2017, **1**, 91.
25 W. C. Chen, Y. Yuan, Y. Xiong, A. L. Rogach, Q. X. Tong and C. S. Lee, *ACS Appl. Mater. Interfaces*, 2017, **9**, 26268.
26 C. Han, G. Xie, H. Xu, Z. Zhang, L. Xie, Y. Zhao, S. Liu and W. Huang, *Adv. Mater.*, 2011, **23**, 2491.
27 X. L. Li, G. Xie, M. Liu, D. Chen, X. Cai, J. Peng, Y. Cao and S. J. Su, *Adv. Mater.*, 2016, **28**, 4614.
28 Y. Li, X. L. Li, D. Chen, X. Cai, G. Xie, Z. He, Y. C. Wu, A. Lien, Y. Cao and S. J. Su, *Adv. Funct. Mater.*, 2016, **26**, 6904.
29 C. Duan, J. Li, C. Han, D. Ding, H. Yang, Y. Wei and H. Xu, *Chem. Mater.*, 2016, **28**, 5667.
30 N. Zhou, S. Wang, Y. Xiao and X. Li, *Chem. – Asian J.*, 2018, **13**, 81.
31 A. Obolda, Q. Peng, C. He, T. Zhang, J. Ren, H. Ma, Z. Shuai and F. Li, *Adv. Mater.*, 2016, **28**, 4740.
32 C. Li, S. Wang, W. Chen, J. Wei, G. Yang, K. Ye, Y. Liu and Y. Wang, *Chem. Commun.*, 2015, **51**, 10632.
33 C. He, H. Guo, Q. Peng, S. Dong and F. Li, *J. Mater. Chem. C*, 2015, **3**, 9942.
34 M. Liu, X. L. Li, D. C. Chen, Z. Xie, X. Cai, G. Xie, K. Liu, J. Tang, S. J. Su and Y. Cao, *Adv. Funct. Mater.*, 2015, **25**, 5190.
35 D. He, Y. Yuan, B. Liu, D.-Y. Huang, C.-Y. Luo, F. Lu, Q.-X. Tong and C.-S. Lee, *Dyes Pigm.*, 2017, **136**, 347.
36 R. Furue, K. Matsuo, Y. Ashikari, H. Ooka, N. Amanokura and T. Yasuda, *Adv. Opt. Mater.*, 2018, **6**, 1701147.
37 S. Chen, Y. Wu, S. Hu, Y. Zhao and D. Fang, *J. Fluoresc.*, 2017, **27**, 451.
38 W. C. Chen, Y. Yuan, S. F. Ni, Q. X. Tong, F. L. Wong and C. S. Lee, *Chem. Sci.*, 2017, **8**, 3599.
39 M. Godumala, S. Choi, H. J. Kim, C. Lee, S. Park, J. S. Moon, K. Si Woo, J. H. Kwon, M. J. Cho and D. H. Choi, *J. Mater. Chem. C*, 2018, **6**, 1160.
40 Y. Yang, S. Wang, Y. Zhu, Y. Wang, H. Zhan and Y. Cheng, *Adv. Funct. Mater.*, 2018, **28**, 1706916.
41 Y. Im, S. Y. Byun, J. H. Kim, D. R. Lee, C. S. Oh, K. S. Yook and J. Y. Lee, *Adv. Funct. Mater.*, 2017, **27**, 1603007.
42 S. Chen, Y. Wu, Y. Zhao and D. Fang, *RSC Adv.*, 2015, **5**, 72009.
43 X. Tang, Q. Bai, Q. Peng, Y. Gao, J. Li, Y. Liu, L. Yao, P. Lu, B. Yang and Y. Ma, *Chem. Mater.*, 2015, **27**, 7050.
44 T. A. Lin, T. Chatterjee, W.-L. Tsai, W.-K. Lee, M.-J. Wu, M. Jiao, K.-C. Pan, C.-L. Yi, C.-L. Chung, K.-T. Wong and C.-C. Wu, *Adv. Mater.*, 2016, **28**, 6976.
45 G. Li, J. Zhao, D. Zhang, J. Zhu, Z. Shi, S. Tao, F. Lu and Q. Tong, *New J. Chem.*, 2017, **41**, 5191.
46 J. Guo, X.-L. Li, H. Nie, W. Luo, S. Gan, S. Hu, R. Hu, A. Qin, Z. Zhao, S.-J. Su and B. Z. Tang, *Adv. Funct. Mater.*, 2017, **27**, 1606458.
47 B. Liu, J. Zhao, C. Luo, F. Lu, S. Tao and Q. Tong, *J. Mater. Chem. C*, 2016, **4**, 2003.
48 K. Wang, F. Zhao, C. Wang, S. Chen, D. Chen, H. Zhang, Y. Liu, D. Ma and Y. Wang, *Adv. Funct. Mater.*, 2013, **23**, 2672.

49 R. Kim, S. Lee, K.-H. Kim, Y.-J. Lee, S.-K. Kwon, J.-J. Kim and Y.-H. Kim, *Chem. Commun.*, 2013, **49**, 4664.
50 W.-C. Chen, G.-F. Wu, Y. Yuan, H.-X. Wei, F.-L. Wong, Q.-X. Tong and C.-S. Lee, *RSC Adv.*, 2015, **5**, 18067.
51 M. J. Frisch, G. W. Trucks, H. B. Schlegel, G. E. Scuseria, M. A. Robb, J. R. Cheeseman, G. Scalmani, V. Barone, B. Mennucci, G. A. Petersson, H. Nakatsuji, M. Caricato, X. Li, H. P. Hratchian, A. F. Izmaylov, J. Bloino, G. Zheng, J. L. Sonnenberg, M. Hada, M. Ehara, K. Toyota, R. Fukuda, J. Hasegawa, M. Ishida, T. Nakajima, Y. Honda, O. Kitao, H. Nakai, T. Vreven, J. A. Montgomery Jr, J. E. Peralta, F. Ogliaro, M. Bearpark, J. J. Heyd, E. Brothers, K. N. Kudin, V. N. Staroverov, R. Kobayashi, J. Normand, K. Raghavachari, A. Rendell, J. C. Burant, S. S. Iyengar, J. Tomasi, M. Cossi, N. Rega, J. M. Millam, M. Klene, J. E. Knox, J. B. Cross, V. Bakken, C. Adamo, J. Jaramillo, R. Gomperts, R. E. Stratmann, O. Yazyev, A. J. Austin, R. Cammi, C. Pomelli, J. W. Ochterski, R. L. Martin, K. Morokuma, V. G. Zakrzewski, G. A. Voth, P. Salvador, J. J. Dannenberg, S. Dapprich, A. D. Daniels, Ö. Farkas, J. B. Foresman, J. V. Ortiz, J. Cioslowski and D. J. Fox, *Gaussian 09, Revision A.02*, Gaussian, Inc., Wallingford CT, 2009.
52 A. D. Becke, *J. Chem. Phys.*, 1993, **98**, 5648.
53 C. Lee, W. Yang and R. G. Parr, *Phys. Rev. B: Condens. Matter Mater. Phys.*, 1988, **37**, 785.